

# Functionalization of Polymer-Wrapped Silver Nanoclusters and Potential Applications as Antimicrobial Mask Materials

Sai Ge, Yamei Han, Manluan Sun, Jianguo Zhao,\* and Guibin Ma\*

Cite This: *ACS Omega* 2023, 8, 42678–42688

Read Online

ACCESS |



Metrics &amp; More

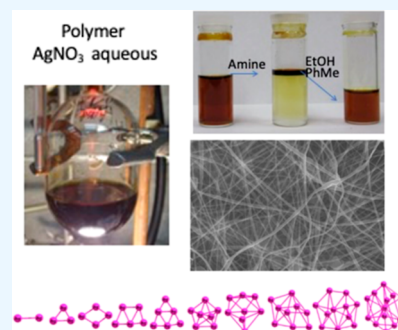


Article Recommendations



Supporting Information

**ABSTRACT:** The poly(methacrylic acid) (PMAA) polymer stabilized silver nanoclusters  $Ag_n$  ( $n = 2-9$ ), synthesized in aqueous solution by the selected light wavelength irradiation photolysis approach, have been functionalized with thiol and amine ligands and successfully transferred from aqueous to organic media. Low- or high-resolution positive mass spectra showed constant species composites with the molecular formula  $Ag_nL_{n-1}$  [ $n = 2$  to  $\sim 9$ ,  $L =$  butylmercaptan ( $C_4H_9S$ ), thiolphenol ( $C_6H_5S$ ), or dodecanethiol ( $C_{12}H_{25}S$ )] and proved that the molecules consist of deprotonated sulfur ligands in each species with one positive charge. Fourier transform infrared and X-ray photoelectron spectroscopy are consistent, indicating deprotonated sulfur, while silver has a zero valence value. The composition of the functionalized silver clusters is in agreement with that observed from polymer-wrapped “naked” silver clusters, which strongly indicates their real existence. For the silver cluster amine systems (heptylamine, dodecylamine, and oleylamine), only “naked” silver cluster species were detected from mass spectroscopy, similar to the polymer-wrapped case, indicating they are not stable enough in the gas phase. The development of a new antibacterial mask material is very important. The dodecylamine-capping silver nanoclusters were selected by coating the coffee filter surface to conduct antibacterial tests with *Staphylococcus aureus* and *Escherichia coli*, demonstrating very efficient antimicrobial properties even with organic capping ligands. Experiments also show that they work on mask material. One nanowire assembly with polystyrene and dodecylamine-capping silver nanoclusters was prepared, showing uniform nanofibers generated via the electrospay technique.



## INTRODUCTION

Nanotechnology is a rapidly developing field due to increased production efficiency and the development of a variety of nanomaterials.<sup>1</sup> Noble-metal nanoclusters (NCs), such as gold and silver, are a fascinating area of contemporary interest in nanomaterials because of their many applications in biology and nanomedicine.<sup>2</sup> The synthesis difficulty arises mainly from the tendency of the strong interaction between the NCs and the aggregate to irreversibly reduce their surface energy. To overcome this issue, strong capping agents with sulfur and nitrogen atoms binding to the cluster surface have been utilized. Regarding Ag/Au metal clusters,  $Au_{11}$ ,<sup>3</sup>  $Au_{13}$ ,<sup>4</sup> and  $Au_{55}$  gold clusters and several new clusters such as  $Au_8$ ,<sup>6</sup>  $Au_{18}$ ,<sup>7</sup>  $Au_{25}$ ,<sup>8</sup> and  $Au_{38}$ ,<sup>9</sup> have been extensively studied, and several of these clusters are considered to be important for biolabeling reagents,<sup>10</sup> fluorescence resonance energy transfer,<sup>11</sup> and for creating luminescent patterns.<sup>12a</sup> Another type of triphenylphosphine-ligand-binding Au cluster has been reported very recently, and it has been shown that hydrogen-containing intermediate Au clusters are responsible for the growth of large Au clusters.<sup>12b</sup>

Studies on silver clusters are relatively rare, but there are some examples of template-assisted syntheses of water-soluble luminescent silver clusters with cores reported in the range from  $Ag_2$  to  $Ag_8$ .<sup>13</sup> However, unlike for gold, there are limited available structural signature data, especially for these very tiny

clusters, and few examples of monolayer-protected silver analogues. Examples of these characterized by mass spectroscopy include one cluster,  $Ag_7(DMSA)_4$  (DMSA: 2,3-dimercaptosuccinic acid), prepared by  $NaBH_4$  reduction, as well as  $Ag_7(H_2MSA)_7$ ,  $Ag_8(H_2MSA)_8$ ,<sup>15</sup> and  $Ag_9(H_2MSA)_7$ <sup>16</sup> ( $H_2MSA$ : mercaptosuccinic acid), prepared by interfacial and solid synthesis routes, respectively.

We have been undertaking silver nanoparticle synthesis, characterization, and applications for a long time, especially in the very concentrated silver nanoparticle system.<sup>17</sup> We have developed a methodology by systematic irradiation with different wavelength light sources and found that we may tailor Ag nanoclusters with a large variety of sizes through the selection of different wavelengths for the photolysis of solutions containing silver nitrate and [poly(methacrylic acid) (PMAA)]. A large series of silver clusters of  $Ag_n$  ( $n = 2-9$ ) are comprehensively identified using mass spectrometry from the light photolysis solution.<sup>18</sup> In addition, after

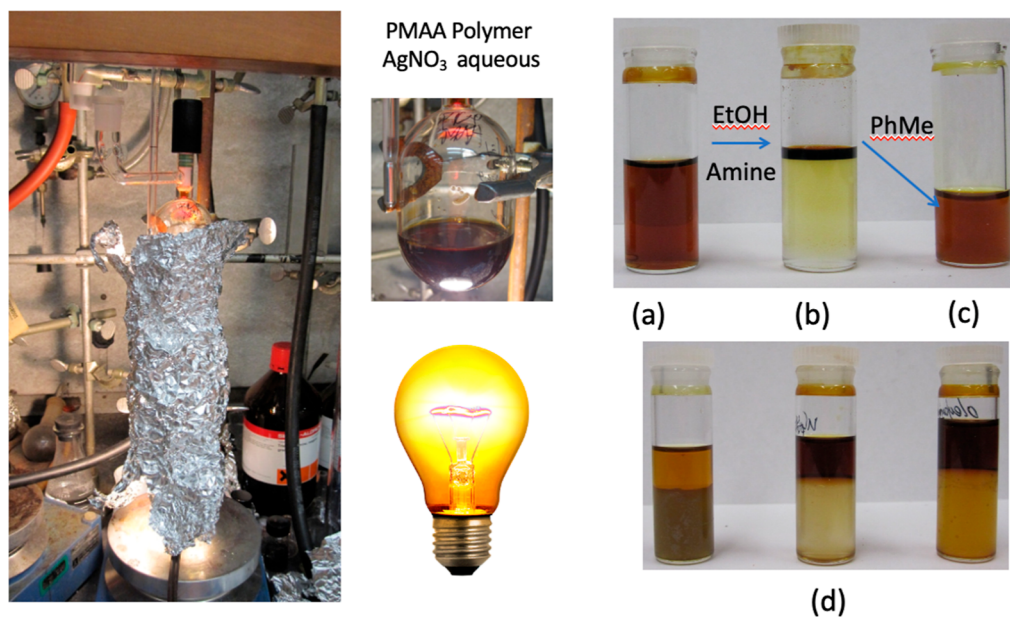
Received: July 26, 2023

Revised: October 12, 2023

Accepted: October 17, 2023

Published: November 3, 2023



Scheme 1. Photolysis Preparation and Functionalization Procedure<sup>a</sup>

<sup>a</sup>Silver nanocluster synthesis: A PMAA polymer and  $\text{AgNO}_3$ -mixed aqueous solution in a round flask was completely sealed by a Teflon septum. The flask was exposed to light, and the flask/light bulb were all covered with aluminum foil for 24 h. Functionalized silver nanoclusters with amine ligands: (d) the phase separation between the aqueous solution and the toluene was not clearly seen for the three selected amine ligands: heptylamine (left), dodecylamine (middle), and oleylamine (right). The pre-addition of ethanol to the aqueous solution of silver nanoclusters and then the addition of dodecylamine resulted in a clear separation between the aqueous solutions and the toluene, as shown in (a), (b), and (c), indicating ethanol support to exchange the organic ligands efficiently and functionalize in a successful way.

assessment of the antimicrobial test, it was found that these generated silver clusters show efficient antimicrobial properties.<sup>18</sup>

Silver metal is considered to have the lowest minimum inhibitory concentration (MIC) of any metal.<sup>19</sup> It has been used as an antimicrobial agent in medicine since antiquity.<sup>20</sup> The antimicrobial property of these tiny silver clusters is greater than that of the large silver nanoparticles, particularly against difficult-to-treat Gram-negative pathogens.<sup>21</sup> With global warming, the microbes surrounding humans become more active and thus threaten human health (e.g., super bacteria and fungus). To eliminate this threat, efficient antimicrobial mask materials are critically important, and further development is essential. These tiny silver nanomaterials without drug resistance are a particularly promising path to achieving this goal.

Current mask materials are hydrophobic polymer-based nanowire materials and generate nanosize to microsize holes in the melt-blown clothes.<sup>22</sup> However, synthesized tiny silver nanoclusters are in an aqueous phase and must make the surface functional with some organic capping ligands to bring the silver nanoclusters to the organic phase. The very tiny silver clusters containing a few numbers of silver metals with organic capping ligands are very difficult to synthesize directly in organic medium, forming mostly large silver nanoparticles.<sup>2b</sup> The tiny silver nanoclusters could only be synthesized in the presence of PMAA polymers in an aqueous solution as both a capping ligand and a photolysis catalyst.<sup>13,17,18</sup> That is why we needed to conduct the synthesis in an aqueous solution and carry out ligand exchange functionalization by thiol and amine organic ligands to bring these tiny silver nanoclusters to the organic phase, permitting us to fabricate the mask antimicrobial materials. Herein, we have systemically conducted further

function of the PMAA polymer-wrapped silver clusters with a series of thiol and amine functional group ligands and fully characterized the structure by multiple techniques (low- or high-resolution mass spectroscopy, UV-vis, and X-ray photoelectron spectroscopy (XPS) spectroscopy). In addition, the functionalized hydrophobic silver nanoclusters have been incorporated into a polymer matrix to generate polymer nanowires, which can be used as antimicrobial materials in mask fabrication.

## EXPERIMENTAL SECTION

**Chemicals and Instrument.** Silver nitrate [ $(\text{AgNO}_3)$  (Aldrich, >99.9%), PMAA] (30% in aqueous sodium solution) ( $M_w = 9500$ ) and polystyrene ( $M_w = 192,000$ ) were purchased from Sigma-Aldrich, St. Louis, MO, United States. A light source was selected for the synthesizing of polymer-wrapped silver nanoclusters (generally 60 W light bulbs with a tungsten metal wire). A JEOL 6301F field emission scanning electron microscope (FESEM) was used with an accelerating voltage of 15 kV, equipped with an energy-dispersive X-ray spectroscopy analysis system (EDA, Bruker model with dual silicon drift detectors), Japan. Mass spectrometry of Applied Biosystems Voyager Elite and a MALDI MS time-of-flight (TOF) mass spectrometer were used to determine the molecular weight properties of all functionalized silver nanocluster solution samples. A pulsed nitrogen laser (337 nm) (3 ns pulse—up to 300  $\mu\text{J}/\text{pulse}$ )-delayed extraction improved the resolution and mass accuracy of the reflectron (ion mirror). High-resolution mass spectra were recorded with a Bruker 9.4 T Apex-Qe FTICR spectrometer operating in the ESI mode. A Cary UV-vis instrument was used to measure the optical properties of all of the functionalized silver nanocluster solution samples.

Bacteria strains: *Escherichia coli* ATCC25922 and *Staphylococcus aureus* ATCC65387; UV Spectrophotometry.

**Synthesis and Functionalization.** Our previous synthesis used a monochromatic light source, and although it is very efficient, it is not suitable for large-scale production. The synthesis of PMAA-wrapped silver nanoclusters in aqueous solution was used in the modified procedure of our previous work.<sup>18</sup> The polymer (PMAA)/silver ion ratio was the same as that in the previous study. However, instead of a monochromatic light source, here, we used a mixed light source from a traditional tungsten metal wire light bulb in a sealed flask (Scheme 1). A sealed flask (volume: 100 mL) filled with 20.0 mL of 5.6 mM aqueous solution with the Ag<sup>+</sup>/monomer (PMAA) molar ratio in 1:1 (5.6 mM AgNO<sub>3</sub> and 5.6 mM monomer concentration of PMAA polymer). Light irradiation in this sealed flask was kept for 24 h to completely incorporate the silver ions in the silver nanoclusters (**Warning:** silver nitrate is used as a precursor in the solution, and this chemical is dangerous and could cause an explosion! It must be handled cautiously, in a small volume, and in low concentration in an isolated location). The organic amine and thiol functionalization procedures are also shown in Scheme 1. The organic ligands, either thiol or amine replacement reactions, in aqueous solutions were not achieved by the direct addition of toluene and selected organic ligands. The phase separation between the aqueous solution and toluene was not clear. The preaddition of ethanol to the aqueous solution of silver nanoclusters, followed by the addition of organic ligands, was successful. The binding reaction and phase separation were then clearly seen, as shown in Scheme 1. This indicates that mixed ethanol/aqueous solutions enhance the organic ligand solubility and allow the efficient completion of the organic ligand replacement reaction, and thus, the functionalization was carried out successfully.

**Electrospray Fabrication Procedure for Silver Nanoclusters inside Nanofibers.** The optimized procedure to assemble silver nanoclusters into nanofibers/nanowires: 0.01 g of dodecylamine capping silver nanoclusters powder was dissolved in 5.0 mL of dimethylformamide (DMF), and then, 1.0 g of polystyrene sphere particles were added with overnight magnetic stirring. This homogeneous solution of polymer nanoclusters was loaded into a plastic syringe and electrospay fabrication of nanofibers under this optimized condition: needle-to-substrate distance of 15 cm, spin rate of 600 rpm, voltage of 15.0 kV, and injection rate of 2.5 mL/h. The thickness of the coating film was controlled by the electrospay time.

**Antimicrobial Test Procedure.** *E. coli* and *S. aureus* were cultured in Luria–Bertani (LB) liquid media at 37 °C, 200 rpm, separately, until the OD<sub>600</sub> value reached 0.8. The silver nanoclusters with dodecylamine capping ligands were dissolved in chloroform and, through the electrospay procedure, coated onto a cellulose coffee filter surface. A piece of coffee filter sheet with a hydrophilic cellulose surface that contained nanomaterials of silver nanoclusters capped with organic dodecylamine ligand was placed above the well bottom of 96 well plates. Then, 180 μL of fresh LB liquid medium well mixed with 20 μL of bacteria culture was added as the experimental group. Meanwhile, wells only containing 20 μL of bacteria and 180 μL of fresh LB liquid media were used as a control group. Bacterial measurements used the spectrophotometer methodology as reported in the literature.<sup>34</sup> At 600 nm absorbance, OD<sub>600nm</sub> is named turbidity, and there is a linear relationship between the concentration (thousand

weight) and absorbance of regular-shaped (approximately spherical) microorganisms, such as bacteria and yeast. The bacterial number *N* can be easily converted based on a linear correlation of OD<sub>600nm</sub> absorbance, according to  $N = 1437.3 \times OD_{600\text{ nm}} - 27.3$  ( $R^2 = 0.998$ ). All measurements were taken in triplicate by taking three different samples and then recording the average values with the standard deviation.

## RESULTS

**Functionalization and Characterization.** Our previous study has demonstrated that it is feasible to generate tiny Ag nanoclusters wrapped by weak oxygen-bonded carboxy polymers of PMAA employing an optimized monomer/Ag<sup>+</sup> ratio and monochromatic UV-light.<sup>18</sup> The “naked” cores of Ag<sub>*n*</sub> nanoclusters ( $n = 2–9$ ) were observed in the gas phase by MALDI mass spectroscopy, which also indicated the existence of weak bonding interactions between the Ag<sub>*n*</sub> nanoclusters and the PMAA polymer chains. In the work presented here, the preparation procedure is modified: instead of monochromatic light, a light bulb is used as the radiation source. Because this light source is readily available, it is suitable for large-scale production.

It is worthwhile to determine the possible methods of functionalizing these tiny nanoclusters by substituting the polymer with a variety of small ligands while avoiding any aggregation. An investigation on the function of this system was conducted, and the final optimized experimental procedures were simple and straightforward (Figure 1). As shown in this figure, for the 1-dodecanethiol ligand, 1 mL of a red aqueous solution of polymer-stabilized Ag<sub>*n*</sub> nanoclusters ( $n$

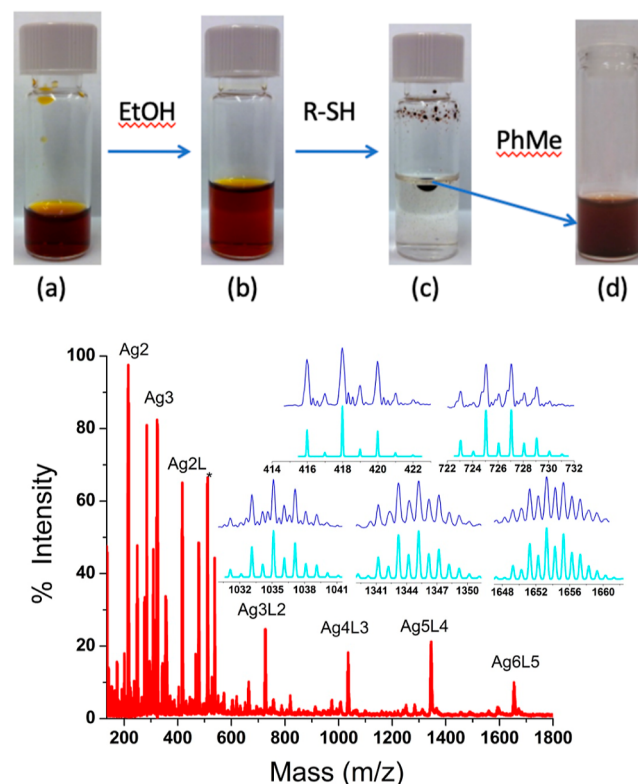


**Figure 1.** MALDI-TOF positive mode mass spectrum (low resolution) of dodecanethiol-functionalized silver nanoclusters. Inset graphs are expanded experimental (blue) and simulated (green) spectra of each individual species.

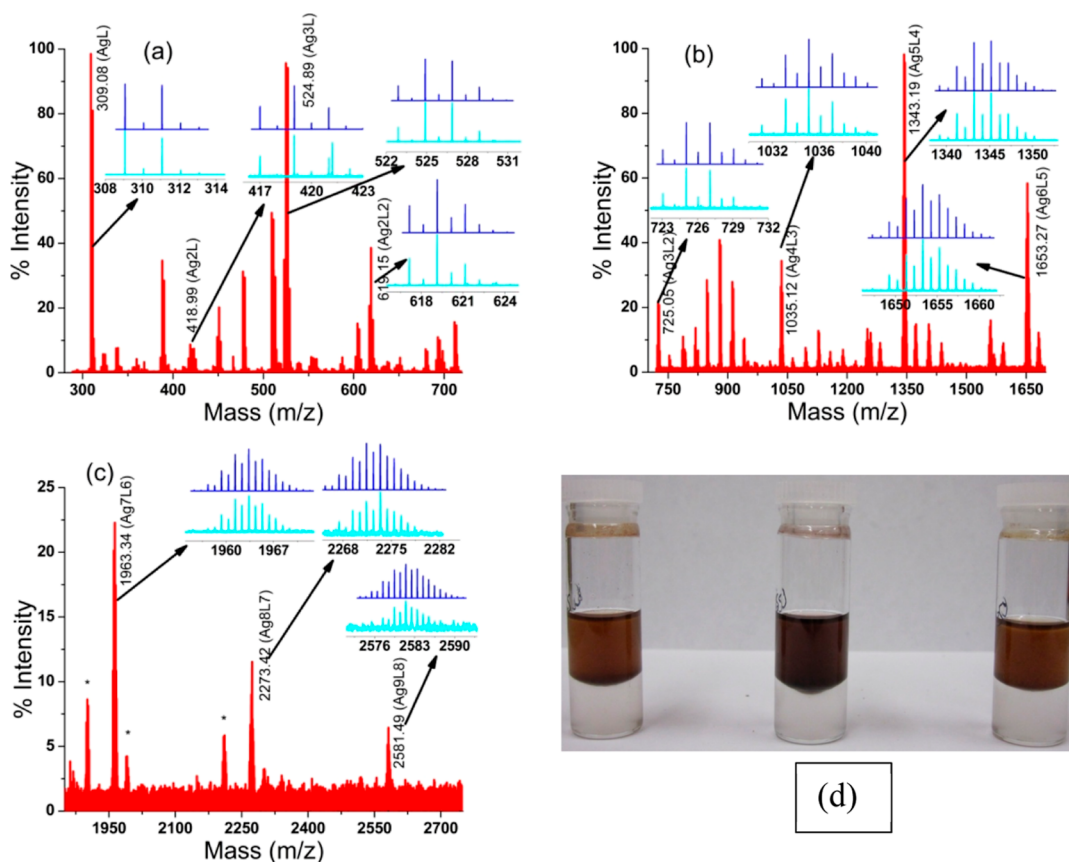


**Figure 2.** ESI positive mode mass spectrum (high resolution) of dodecanethiol-functionalized silver nanoclusters. (a) Plot range of 300–725  $m/z$ ; (b) plot range of 725–1650  $m/z$ ; (c) plot range of 1850–2750  $m/z$ . Inset traces in (a), (b), and (c) are expanded experimental (blue) and simulated (green) spectra of each individual species. (d) phase separation of the functionalized Ag nanoclusters, butylmercaptan (left), thiophenol (middle), and dodecanethiol (right).

= 2–9) (a) was mixed with a 1:1 volume ratio of ethanol (b), and 0.2 mL of 1-dodecanethiol liquid was added to the solution (b). After shaking for 5 min, the red color faded and the crude black-oil liquid came out during this period (c). The black crude liquid was isolated by decantation of the colorless solution and then dissolved in a 1:1 volume ratio of ethanol and toluene, and a red-colored homogeneous solution (d) was generated. Through three steps, the Ag nanoclusters were successfully transferred from an aqueous solution to the mixed organic solvents. The red color of (d) is strong evidence indicating that the Ag nanoclusters have been functionalized by 1-dodecanethiol ligands.

The species composition of solution (d) was analyzed by employing MALDI positive mass spectroscopy. From low-resolution MALDI, the ligand-free  $\text{Ag}_2$ ,  $\text{Ag}_3$ , and 1-dodecanethiol ( $\text{C}_{12}\text{H}_{26}\text{S}$ :  $\text{CH}_3-(\text{CH}_2)_{11}-\text{SH}$ )-bonding series of  $\text{Ag}_2(\text{C}_{12}\text{H}_{25}\text{S})$  ( $m/z = 418.99$ ),  $\text{Ag}_3(\text{C}_{12}\text{H}_{25}\text{S})_2$  ( $m/z = 725.05$ ),  $\text{Ag}_4(\text{C}_{12}\text{H}_{25}\text{S})_3$  ( $m/z = 1035.15$ ),  $\text{Ag}_5(\text{C}_{12}\text{H}_{25}\text{S})_4$  ( $m/z = 1343.19$ ), and  $\text{Ag}_6(\text{C}_{12}\text{H}_{25}\text{S})_5$  ( $m/z = 1653.27$ ) were observed and can be assigned with the simulated isotopic patterns (Figure 1). A few very small peaks were observed in the high mass region ( $m/z = 1900$ – $2700$ ), but it was hard to assign them in comparison to the simulated isotopic patterns. High-resolution ESI positive mass spectroscopy for this sample was performed. Apart from the identified species from low resolution spectroscopy, three other species,  $\text{Ag}_7(\text{C}_{12}\text{H}_{25}\text{S})_6$  ( $m/z = 1973.34$ ),  $\text{Ag}_8(\text{C}_{12}\text{H}_{25}\text{S})_7$  ( $m/z = 2273.42$ ), and  $\text{Ag}_9(\text{C}_{12}\text{H}_{25}\text{S})_8$  ( $m/z = 2581.49$ ), are clearly seen in the high

mass region (Figure 2b,c). In addition, three low-mass species,  $\text{Ag}(\text{C}_{12}\text{H}_{25}\text{S})$  ( $m/z = 309.08$ ),  $\text{Ag}_3(\text{C}_{12}\text{H}_{25}\text{S})$  ( $m/z = 524.89$ ), and  $\text{Ag}_2(\text{C}_{12}\text{H}_{25}\text{S})_2$  ( $m/z = 619.15$ ), were identified in the simulated species isotopic patterns (Figure 2a). The unexpected result, observed from both low- and high-resolution mass spectra, is that the sulfur-bonded proton is not observed in the detected mass peaks. It may be that protons that are weakly bonded to sulfur are easily dissociated in the formed nanoclusters. However, Fourier transform infrared (FTIR) also showed there is no S–H vibration band, expected to appear around  $2500\text{ cm}^{-1}$  (Figure S1). Another possibility is that the two S–H groups can easily form an S–S bond and through it bond to the silver metals. Interestingly, the detected formula masses of the functionalized species all match  $\text{Ag}_n\text{L}_m$  ( $n = m + 1$ ) compositions, which are probably the most stable naturalized compositions.

1-Dodecanethiol as a functional group has been shown to be ideal for replacing the polymer and generating new formula species attached to the tiny Ag nanoclusters. Next, in comparison, we investigated what happens with a relatively short carbon chain thiol ligand. Butyl mercaptan ( $\text{C}_4\text{H}_{10}\text{S}$ :  $\text{CH}_3-\text{CH}_2-\text{CH}_2-\text{CH}_2-\text{SH}$ ) was selected, and a similar functional procedure was used. As butyl mercaptan liquid was dropped into solution b, instead of formatting a suspension of crude black liquid, a black precipitate formed at the bottom. We noticed that the reaction formed the black precipitate within a few minutes, but it took a few hours for the precipitate to completely fall to the bottom, and it tended to

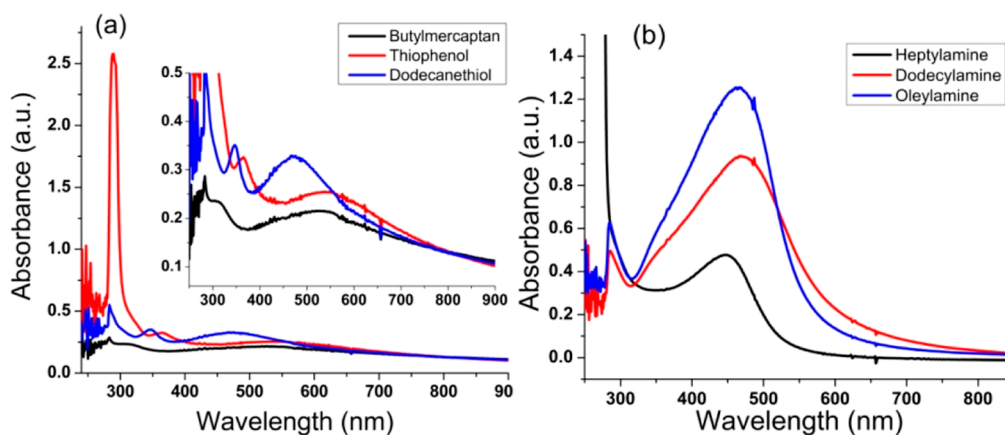


**Figure 3.** UV-vis spectra of (a) thiol and (b) amine for the three thiol and three amine ligands, as shown in inset captions.

stick to the glass wall (Figure S2). The isolated precipitate can be dissolved in 1:1 ethanol/toluene. As expected, an identical composition result as 1-dodecanethiol was seen from MALDI positive mass spectroscopy; the species  $\text{Ag}_2(\text{C}_4\text{H}_9\text{S})$  ( $m/z = 304.85$ ),  $\text{Ag}_3(\text{C}_4\text{H}_9\text{S})_2$  ( $m/z = 500.80$ ),  $\text{Ag}_4(\text{C}_4\text{H}_9\text{S})_3$  ( $m/z = 698.75$ ),  $\text{Ag}_5(\text{C}_4\text{H}_9\text{S})_4$  ( $m/z = 894.69$ ),  $\text{Ag}_6(\text{C}_4\text{H}_9\text{S})_5$  ( $m/z = 1092.64$ ), and  $\text{Ag}_7(\text{C}_4\text{H}_9\text{S})_6$  ( $m/z = 1290.59$ ) were detected from the low-resolution spectroscopy (Figure S3), and additional species of  $\text{Ag}_8(\text{C}_4\text{H}_9\text{S})_7$  ( $m/z = 1486.54$ ) and  $\text{Ag}_9(\text{C}_4\text{H}_9\text{S})_8$  ( $m/z = 1684.49$ ) were seen from high-resolution ESI positive mass spectra (Figure S4). Also, it matches the species formula  $\text{Ag}_n\text{L}_m$  ( $n = m + 1$ ) with a deprotonated sulfur present in the generated species.

It is possible to do the ligand exchange and phase separation at the same time for these three thiol ligands. As the thiol ligand was added into a 1:1 ethanol/aqueous silver nanocluster solution and the same volume of toluene was added in the meantime, the ligand exchange reaction and phase separation finished under stationary conditions within a few minutes after shaking for 1 min (Figure 2d). The dark red color moved from the bottom aqueous layer to the top toluene layer, indicating that the thiol ligand-functionalized Ag nanoclusters were extracted to the organic phase.

So far, we have demonstrated that long-chain 1-dodecanethiol and short-chain butyl mercaptan are all excellent ligands to functionalize the PMAA polymer-wrapped tiny silver nanoclusters. Thereafter, we conducted functionalization with an aromatic thiol ligand of thiophenol. The functionalization reaction and phase separation were slower than those for 1-dodecanethiol and butyl mercaptan. The precipitate was red-brown, and it can be dissolved in either 1:1 ethanol/toluene or toluene; however, the solution is not stable enough, and precipitation happens while keeping it stationary, but it can redissolve with shaking. The MALDI positive mass spectra showed the species  $\text{Ag}_2(\text{C}_6\text{H}_5\text{S})$  ( $m/z = 324.82$ ),  $\text{Ag}_3(\text{C}_6\text{H}_5\text{S})_2$  ( $m/z = 540.73$ ),  $\text{Ag}_4(\text{C}_6\text{H}_5\text{S})_3$  ( $m/z = 758.65$ ),  $\text{Ag}_5(\text{C}_6\text{H}_5\text{S})_4$  ( $m/z = 974.56$ ),  $\text{Ag}_6(\text{C}_6\text{H}_5\text{S})_5$  ( $m/z = 1192.48$ ), and  $\text{Ag}_7(\text{C}_6\text{H}_5\text{S})_6$  ( $m/z = 1410.40$ ) from the low-resolution spectroscopy (Figure S5), and two other additional species of  $\text{Ag}_8(\text{C}_6\text{H}_5\text{S})_7$  ( $m/z = 1626.31$ ) and  $\text{Ag}_9(\text{C}_6\text{H}_5\text{S})_8$  ( $m/z = 1844.24$ ) were seen from the high-resolution ESI positive mass spectra (Figure S6).

Three types of thiol ligands have been applied to functionalize the polymer-wrapped silver nanoclusters in mixed ethanol and aqueous solutions, and the generated new hydrophobic-ligand-bound silver nanocluster species are liable

to isolate from the aqueous medium and to distribute easily into organic solvents. The functionalized new species had identical compositions for both silver cores and binding numbers with the three ligands, and all match the molecular formula  $(\text{Ag})_n(\text{L})_{n-1}$  ( $n = 2-9$ ,  $\text{L} = \text{C}_4\text{H}_9\text{S}$ ,  $\text{C}_{12}\text{H}_{25}\text{S}$ , and  $\text{C}_6\text{H}_5\text{S}$ ) in the detected gas phase. The species in solution are probably the same formula as in the gas phase because of an identical composition result observed from three different types of ligands, indicating that the species composition is very stable. The sulfur is considered a soft coordination ligand, and it bonds strongly to the soft silver metal, but it is more toxic. The nitrogen-containing ligand is harder than thiol but less toxic. When considering potential applications of these functionalized tiny silver nanoclusters in antibacterial and antflammable medicine or biological systems, the selection of less toxic functional groups is of critical importance. For a wide variety of possibilities to functionalize these silver nanoclusters to meet different required purposes, oleylamine ( $\text{CH}_3(\text{CH}_2)_7\text{CH}=\text{CH}(\text{CH}_2)_7\text{CH}_2\text{NH}_2$ ) was used to prepare its bonding silver nanocluster species in situ. As oleylamine was added to the 1:1 ethanol/aqueous mixed solution, it became a glutinous solution upon shaking for a couple minutes. Eventually, it became two phases with a clear interface after being held stationary for approximately 1 h (as shown in Scheme 1d). The top dark-red liquid can be nicely distributed in 1:1 ethanol/toluene after phase separation. The same procedure failed for the other two amine ligands, e.g., heptylamine and dodecylamine. When solid dodecylamine was directly added to the 1:1 ethanol/aqueous solution, a black solid was obtained, and it could not be dissolved again. However, it worked fine when dodecylamine-dissolved ethanol was added to the same volume of silver nanoclusters aqueous solution and extracted by toluene immediately. This procedure was applied with heptylamine (Scheme 1a-c). Because heptylamine has a shorter carbon chain than the other two amine ligands, dodecylamine and oleylamine, the phase separation did not occur spontaneously, and the lightly red color of the top toluene indicated that the species were not completely extracted into the organic phase (Scheme 1d left bottle).

MALDI positive mass showed that the results were unlike those for the thiol silver nanocluster species; instead of observing amine-Ag nanocluster species, the “naked”  $\text{Ag}_n$  nanoclusters ( $n = 2-9$ ) were seen in the mass spectra, indicating the amine-binding silver nanocluster species was not stable enough in the gas phase. The identical result for silver

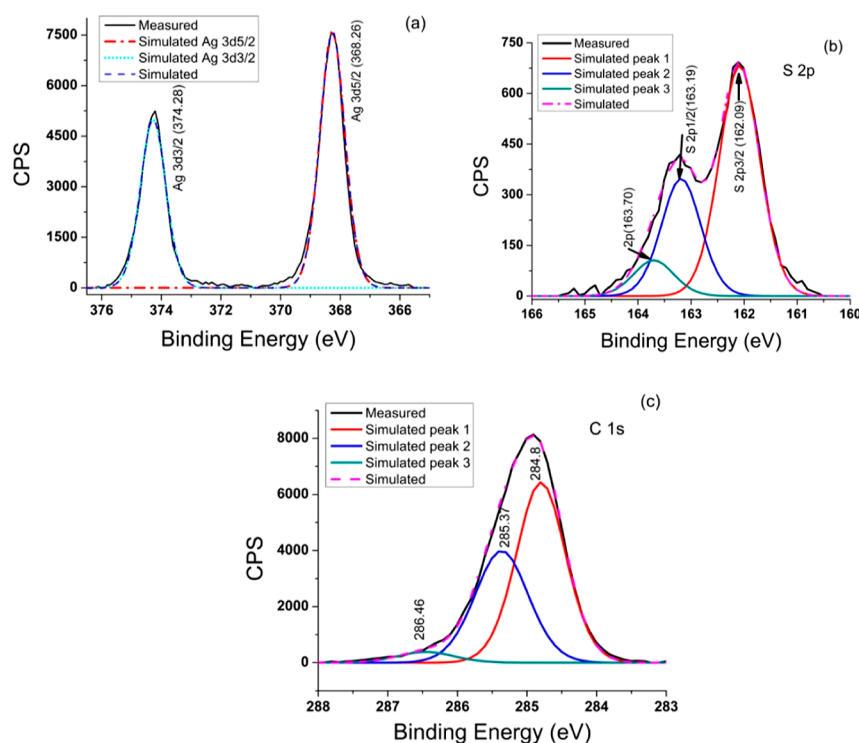


**Figure 4.** XPS spectra of solid 1-dodecanethiol-functionalized silver nanoclusters. (a) Ag 3d, (b) S 2p, and (c) C 1s.

core species was observed as the precursor solution of the carboxyl group bonding the PMAA polymer system discussed previously.<sup>18</sup> This result is expected since nitrogen and oxygen ligands are weaker binding ligands to silver nanoclusters than are sulfur binding ones, and it seems not stable enough in the gas phase. Yet, the FTIR spectra of the free dodecylamine and the dodecylamine-capped silver nanoclusters show different vibration bands, indicating that the dodecylamines are truly binding to the silver nanoclusters in the solid phase (Figure S1). The colorful silver nanoclusters were transferred from the aqueous solution to the organic phase by selected amine ligands, which also indicated that these amine ligands were binding to silver nanoclusters. Perhaps the capped ligand forms the covalent bond for Ag–S and not for Ag–N, which is more probable because it has more ionic bond character and ease of dissociation in the gas phase.

**UV–vis Spectra and XPS.** Broad absorbance bands in UV–vis spectra of three thiol-functionalized Ag nanoclusters appeared at 533, 553, and 472 nm with narrow peaks at 317, 365, and 347 nm for butylmercaptan, thiophenol, and dodecanethiol, respectively (Figure 3a). In accordance with the previous studies on silver clusters,<sup>18</sup> we assign the broad peaks to interband transitions between orbitals derived from the 4d valence band and 5 sp conduction band. Typically, templated Ag<sub>n</sub> clusters and monolayer-protected clusters show interband transitions between 400 and 600 nm,<sup>13,32</sup> which are in good agreement with our observed data. The narrow peaks are assigned to ligand-to-metal core charge transfer (LMCT) absorbance.<sup>33</sup> Each thiol ligand localizes an electron from the delocalized metallic core of the clusters, and this ligand-to-metal core interaction has previously been demonstrated by DFT calculations.<sup>33c</sup> Thiophenol contains a conjugated phenyl group, and thus, the electron density of its bound silver cluster core is more delocalized; the red-shift of the absorbance bands is obvious in appearance in this functionalized system. An

additional strong peak at 288 nm for thiophenol (C<sub>6</sub>H<sub>5</sub>–S–) is due to  $\pi$  to  $\pi^*$  transitions for the phenyl group of the thiol ligand (C<sub>6</sub>H<sub>5</sub>–). Absorbance bands for the selected amine ligands of the silver nanoclusters appear at 447, 467, and 466 nm, respectively, for heptylamine, dodecylamine, and oleylamine in solution (Figure 3b). Compared with the thiol system, only one broad band is seen, consistent with the absorbance band seen from polymer-wrapped Ag<sub>n</sub> nanoclusters through the oxygen-coordinated PMAA. A correlation of absorbance values with carbon chain lengths is seen in both the thiol and amine systems, but big differences are seen for the amine ligands. All these solutions are prepared under the same conditions, and the only difference is the ligands used. It may be that the carbon chain lengths of the ligands affect the phase transfer forces, resulting in different silver nanocluster concentrations for the organic phases. It is reasonable that long carbon chain ligands have more phase transfer drive forces and thus may transfer relatively more silver nanoclusters than short carbon chain ligands because, in principle, the absorbance intensity is proportional to the silver nanocluster concentration.

In the functionalization preparation, it was noticed that the phase separation for the three selected thiol ligands is fast and complete (Figure 2d), but that for the selected amine ligands is quite slow, and there seems to be an equilibrium phase distribution (Scheme 1d) since after 2 days, the red color of the aqueous phase is still apparent, indicating the presence of some silver nanocluster species in that phase. However, it can be seen that the color depth in the top organic phase is proportional to the carbon chain length (Scheme 1d, bottom from left to right). This is understandable considering that the amine group is hydrophilic and the carbon chain is hydrophobic. Since the amine–NH<sub>2</sub> group in the three ligands is the same, the hydrophilic force is constant, but the hydrophobic force increases as the carbon chain length

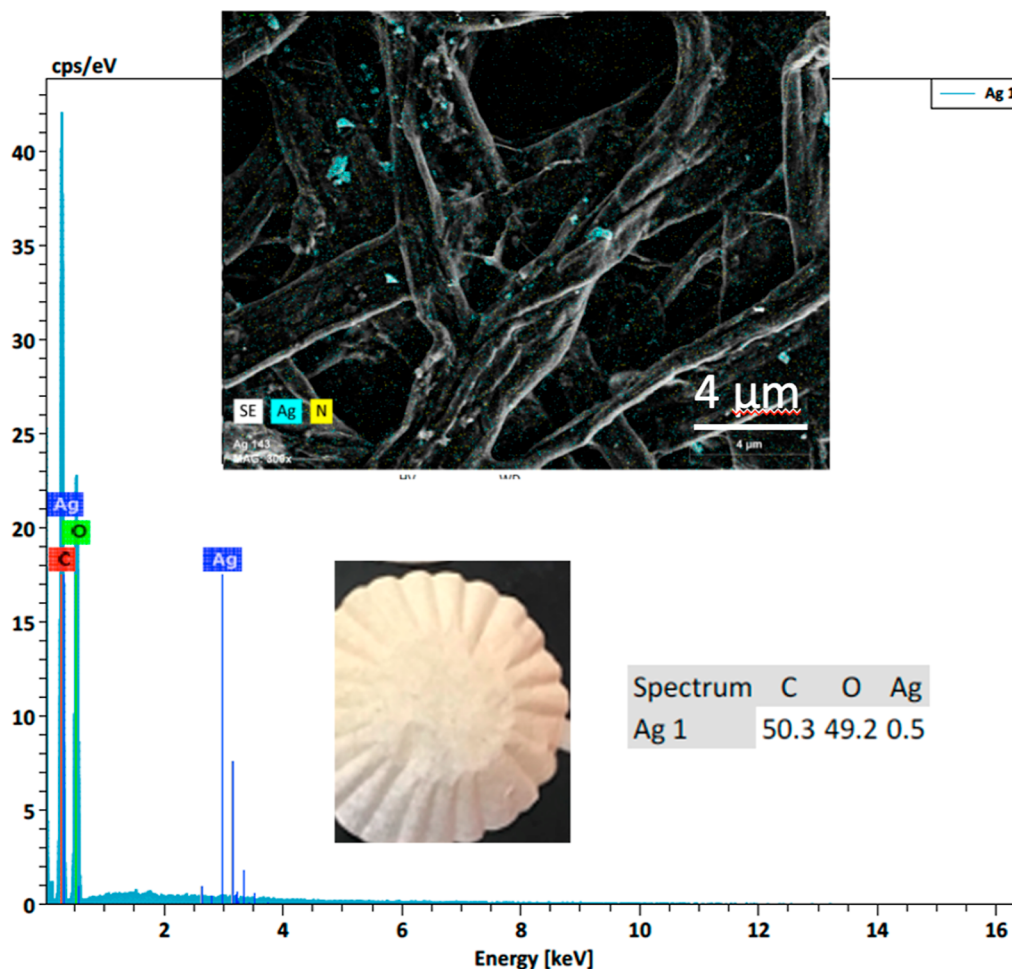


**Figure 5.** SEM/EDS characterization of electro spray-coated dodecylamine-capped silver nanoclusters on the coffee filter surface.

increases. As expected, the long carbon chain amine ligands of dodecylamine and oleylamine transfer not only more species but also larger silver nanoclusters to the organic phase compared with the relatively small heptylamine. These results are consistent with the UV–vis absorbance spectra (Figure 3b), showing large absorbance values for long-chain ligands. Considering the sulfur and nitrogen ligands in silver clusters, the sulfur–Ag bond is a covalent bond, while the nitrogen–Ag bond tends to be ionic, similar to the oxygen–Ag bond. Only covalent bonds are stable in the gas phase, and LMCT can also be detected from the UV–vis spectroscopy, as discussed in a previous text.

More information about the system, such as the molecular formula and the oxidation state of silver, is provided by XPS. XPS survey spectra show the expected elements Ag, C, and S. Ag 3d (Figure 4a) shows an Ag<sup>0</sup> value (3d(S/2) 368.26 eV) that is consistent with the average values of Ag metal reported in the literature (average value: 368.20 ± 0.1).<sup>23a</sup> S 2p is thiolate-like,<sup>23</sup> with values of 162.09 eV observed for 2p(3/2) and 163.19 eV for 2p(1/2), with an intensity ratio of 2:1 (Figure 4b). However, as we fit the measured intensity of the peak, it fits well but introduces an additional broad peak at a value of 163.70 eV, indicating two types of S in the sample. This is in agreement with the FTIR and mass spectra, both of which suggest the loss of the thiolate proton on the thiol-functionalized Ag clusters. From the formula Ag<sub>n</sub>L<sub>n-1</sub>, one may expect that the Ag coordinated to S has two possibilities, either

even or odd; this is consistent with the peak intensity simulation, but the additional introduced peak indicates that the S is not identical at even and odd numbers for the cluster species. The interaction between Ag and S in our system is similar to that for AuO<sub>2</sub> clusters reported in the literature.<sup>23b</sup> Only one carbon peak is seen (Figure 4c), indicating that the cluster composition is constant. However, as we fit the observed peak intensity, three peaks at 284.8, 285.37, and 285.46 eV are generated, which indicates that the ligand binding to the metal surface causes the carbon chain to be in a slightly different environment. The carbon with a relatively high binding energy is more likely to be close to the metal surface, which is consistent with the data in the literature.<sup>23a</sup>

**Antimicrobial Test Results.** *S. aureus* (Gram-positive) is one of the most common causes of epidemic infection and is frequently found in the upper respiratory tract and on the skin.<sup>24</sup> Antimicrobial property against *S. aureus* was assessed in our previous work with silver nanoclusters in an aqueous solution wrapped in PMAA as the antimicrobial agent. It significantly reduced the viable cell count to close to the limit of detection (<0.0001).<sup>18</sup> Thus, we asked ourselves, do these silver nanoclusters still show antimicrobial capability after organic capping ligand functionalization? The silver nanoclusters capped with dodecylamine were selected to conduct antimicrobial tests. It was challenging because the bacteria are in the aqueous phase and the organically functionalized silver nanoclusters are only dissolved in organic solvents, such as

chloroform. In such cases, the organic phase of dodecylamine-stabilized silver nanoclusters was coated onto cellulose coffee filter paper surface fiber matrices by an electrospray technique. The filter paper has a hydrophilic surface, and the aqueous bacteria can access the coffee filter paper surface where the silver nanoclusters are located. The SEM/EDS/mapping characterization of the coffee filter paper surface via electrospray fabrication with organic capping silver nanoclusters is shown in Figure 5. People are also easily infected with pathogenic *E. coli*, which is widely distributed in the environment as well as in our bodies. Urinary tract infection, meningitis, and diarrhea are also common diseases caused by *E. coli*.<sup>25</sup> Hence, these two kinds of bacteria were selected and used to investigate the antibacterial ability of our organic ligand-functionalized silver cluster nanomaterial. The details of the procedure are described in the Experimental Section. Compared to the control group, the nanomaterial presented excellent antibacterial activity against both bacteria. The highest antibacterial rate was 82.16% for *E. coli* and 77.66% for *S. aureus*, as shown in Figure 6. This confirms that the

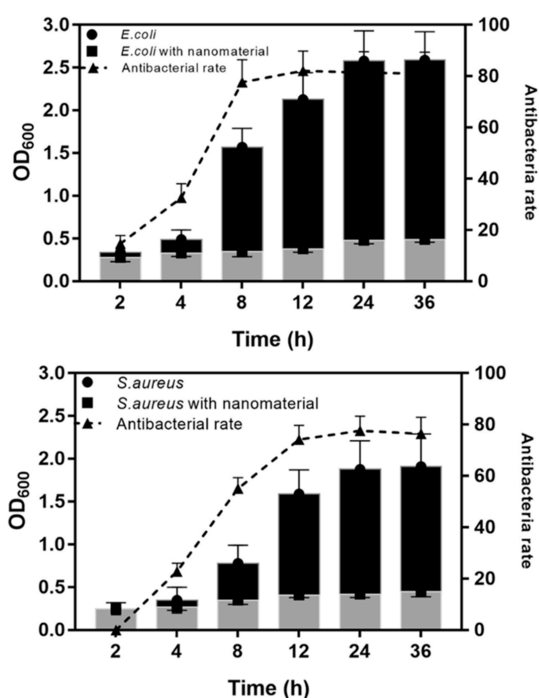


**Figure 6.** Antibacterial test results for dodecylamine-capped silver nanoclusters against *E. coli* and *S. aureus*. The OD<sub>600</sub> converted to the number of bacteria by  $N_{(\text{number})} = 1437.3 \times \text{OD}_{600 \text{ nm}} - 27.3$  ( $R^2 = 0.998$ ).<sup>34</sup>

organic dodecylamine-capped silver nanoclusters also show excellent antimicrobial activity, and hence, organic ligand capping does not affect the silver nanocluster core antimicrobial activity.

**Silver Nanoclusters Nanofiber Fabrication and SEM Characterization.** Polystyrene sphere particles are synthetic polymers made from monomers of the aromatic hydrocarbon styrene. It is a transparent, inexpensive resin, has a poor barrier to oxygen and water vapor, has a low melting point, and is one of the most widely used plastics.<sup>35</sup> It can be fabricated easily as nanofibers, and it is a good candidate material for next-generation masks. In a dimethylformamide solvent, a homogeneous, clear solution of both dodecylamine-capped

silver clusters and polystyrene was generated at room temperature. Under optimized conditions, the fiber sheet on the aluminum foil surface was fabricated via an electrospray technique. SEM images have demonstrated that long nanowires are formed, and silver nanoclusters are also present in these nanowires (EDS indicated 96.5% carbon and 3.5% silver from the selected area) (Figure 7). Elemental mapping of the selected fiber area clearly shows that a small amount of silver metal is homogeneously distributed throughout the carbon-base polymer nanowire phase. This demonstrates that the fabrication of homogeneous polymer nanowires containing organic dodecylamine-capped silver nanoclusters is feasible.

## DISCUSSION

The increasing global threat of microbial activities has stimulated us to explore highly efficient health care protection materials. A variety of different approaches have been developed to incorporate antimicrobial composite materials to mask surfaces via surface chemical modifications, such as surface functionalization with antimicrobial substances<sup>26</sup> and salt coating<sup>27</sup> to improve their performance. Silver has been used as an antimicrobial reagent for a long time in medicine due to its highly efficient antimicrobial properties and low toxicity.<sup>17,18</sup> We have recently developed a facile approach to generating very high antimicrobial performance silver nanoclusters in aqueous solutions by monochromatic photolysis.<sup>18</sup> Herein, we have updated the photolysis using a light bulb source and a further methodology to functionalize with organic thiol and amine ligands to bring these tiny silver nanoclusters into the organic phase without any structural change. It has also been shown that the organic ligand-capped silver nanoclusters maintain their antimicrobial properties. Thus, these may be used as an organic polymer-phase antimicrobial agent. After the selected dodecylamine-capped silver nanoclusters and polystyrene were placed in dimethylformamide, we successfully incorporated these silver nanoclusters into polymer nanofibers or nanowires to demonstrate the possibility of incorporating these antimicrobial silver nanoclusters in a polymer phase for application as multiple-use mask material.

Nanotechnology is rapidly expanding due to the increase in nanomaterial designs and syntheses on very small (1–100 nm) scales. A large number of the nanomaterials presently used in consumer products are metal-based nanoparticles (NPs), including Ag<sup>+</sup>, Cu<sup>+</sup>, Ti<sup>2+</sup>, Zn<sup>2+</sup>, and Au<sup>+</sup>. Silver (Ag) NPs are the most widely used due to their unique physicochemical properties and bactericidal functions, as well as their low manufacturing cost.<sup>28</sup> The antibacterial effects of silver salts were first reported in 1857 by Dr. J. Marion Sims.<sup>29</sup> A major step forward in Ag technology was the introduction of solid nanocrystalline silver (NCS) dressings in the late 1990s.<sup>30</sup> There are at least 315 consumer products that contain Ag NPs in the Woodrow Wilson database, including clothing, personal care products, wound dressings, teddy bears, washing machines, and air purifiers.<sup>31</sup> We have recently developed a photolysis synthesis method to generate maximum cluster species and concentrations of silver nanocluster mixtures in aqueous solutions<sup>18</sup> that show the lowest MIC of any metal nanoparticles. These very tiny silver atomic clusters have bridging properties between those of atomic silver and those of NCS. Herein, we have expanded the synthesis procedure of these silver nanoclusters using a light bulb light source and further functionalized them with organic ligands to bring these silver nanoclusters to the organic phase with either thiol or

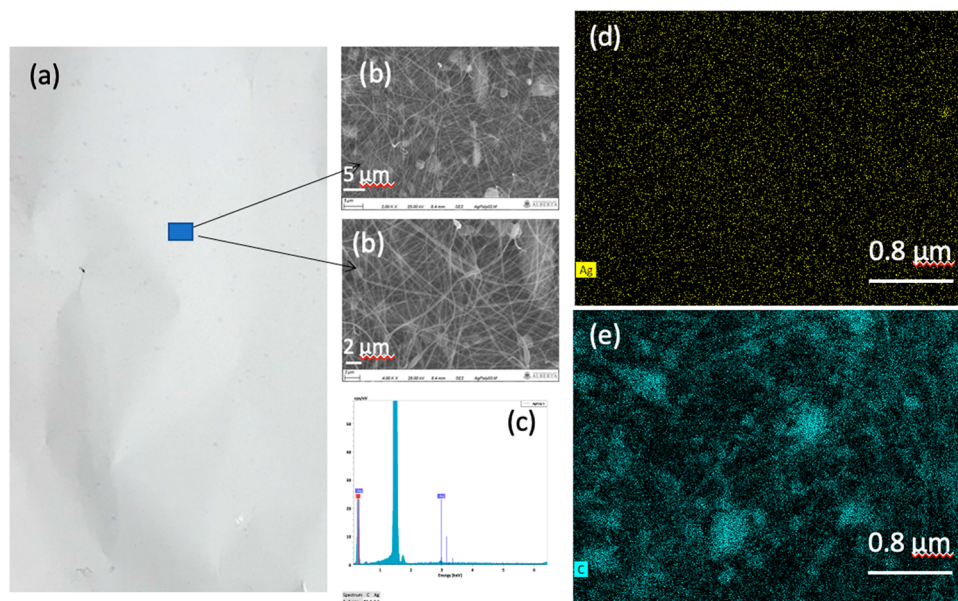


**Figure 7.** SEM images and characterization of polymer nanowire fiber sheets containing dodecylamine-capped silver nanoclusters prepared by electro spray fabrication. (a) Fiber sheet, (b) SEM images of the fiber sheet, (c) EDS of the fiber sheet, (d) silver mapping image, and (e) carbon mapping image.

amine ligands. We demonstrated through an antibacterial test and nanofiber fabrication that these silver nanoclusters can be used as antimicrobial mask materials. A new milestone for silver metal nanomaterial application has been achieved in this work, which expands to a novel application system.

## CONCLUSIONS

In conclusion, we have conducted the functionalization of PMAA polymer-wrapped tiny “naked” silver clusters using a series of thiol (R-SH) and amine (R-NH<sub>2</sub>) functional group ligands. Our experimental results show the developed approach here is feasible, so it opens a novel route to synthesize these tiny silver nanoclusters in organic solvents through samples generated by reduced reagent-free photolysis in aqueous solutions. The full structural characterization results from mass spectrometry demonstrate that the preparation of silver nanocluster species formed by binding with organic ligands is simple and straightforward. One dodecylamine-capped silver nanocluster was selected and deposited on a hydrophilic cellulose coffee filter paper to test the antimicrobial properties; our observed results show that it remains an efficient antimicrobial agent even if it is presently considered a nonwater-soluble species. These organic-capped silver nanoclusters can be easily incorporated into hydrophobic mask polymer materials and potentially used as antimicrobial mask materials for the manufacture of multiple-use masks to relieve the environmental pressure resulting from discarded masks, a clear benefit to the global environment.

## ASSOCIATED CONTENT

### Supporting Information

The Supporting Information is available free of charge at <https://pubs.acs.org/doi/10.1021/acsomega.3c05454>.

FTIR spectra, additional ESI mass spectra, and functionalization separation details for other organic ligands (PDF)

## AUTHOR INFORMATION

### Corresponding Authors

**Jianguo Zhao** – Engineering Research Center of Coal-based Ecological Carbon Sequestration Technology of the Ministry of Education, Shanxi Datong University, Datong, Shanxi Province 037009, PR China; Key Laboratory of National Forest and Grass Administration for the Application of Graphene in Forestry, Shanxi Datong University, Datong, Shanxi Province 037009, PR China; Email: [jgzhaoshi@126.com](mailto:jgzhaoshi@126.com)

**Guibin Ma** – Engineering Research Center of Coal-based Ecological Carbon Sequestration Technology of the Ministry of Education, Shanxi Datong University, Datong, Shanxi Province 037009, PR China; Department of Chemistry, University of Alberta, Edmonton, Alberta T6G 2G2, Canada; [orcid.org/0000-0002-9920-7153](https://orcid.org/0000-0002-9920-7153); Email: [guibin@ualberta.ca](mailto:guibin@ualberta.ca)

### Authors

**Sai Ge** – Engineering Research Center of Coal-based Ecological Carbon Sequestration Technology of the Ministry of Education, Shanxi Datong University, Datong, Shanxi Province 037009, PR China; Key Laboratory of National Forest and Grass Administration for the Application of Graphene in Forestry, Shanxi Datong University, Datong, Shanxi Province 037009, PR China

**Yamei Han** – Engineering Research Center of Coal-based Ecological Carbon Sequestration Technology of the Ministry of Education, Shanxi Datong University, Datong, Shanxi Province 037009, PR China; Key Laboratory of National Forest and Grass Administration for the Application of Graphene in Forestry, Shanxi Datong University, Datong, Shanxi Province 037009, PR China

**Manluan Sun** – Engineering Research Center of Coal-based Ecological Carbon Sequestration Technology of the Ministry of Education, Shanxi Datong University, Datong, Shanxi Province 037009, PR China; Key Laboratory of National Forest and Grass Administration for the Application of

Graphene in Forestry and School of Chemistry and Chemical Engineering, Shanxi Datong University, Datong, Shanxi Province 037009, PR China

Complete contact information is available at:

<https://pubs.acs.org/10.1021/acsomega.3c05454>

## Notes

The authors declare no competing financial interest.

## ACKNOWLEDGMENTS

This work was performed at the Engineering Research Center of Coal-based Ecological Carbon Sequestration Technology of the Ministry of Education, Shanxi Datong University, and was supported by Foundation items: the National Natural Science Foundation of China (52071192), the Shanxi 1331 project foundation for graphene industrialization application technology of collaborative innovation center, the Shanxi new carbon functional materials engineering research center, the Shanxi Science and Technology Major Project (20181102003), the Shanxi Science and Technology Achievements Transformation Guide Project (201804D131041), the Science and Technology Innovation Project of Universities in Shanxi Province (2019L0773 and 2019L0771), and the Shanxi Province Science Foundation for Youths (20210302124435 and 202103021223339). The authors thank Guy Bernard for his helpful comments.

## REFERENCES

- (1) (a) Baig, N.; Kammakam, I.; Falath, W. Nanomaterials: a review of synthesis methods, properties, recent progress, and challenges. *Mater. Adv.* **2021**, *2*, 1821–1871. (b) Kolahalam, L. A.; Kasi Viswanath, I.; Diwakar, B. S.; Govindh, B.; Reddy, V.; Murthy, Y. L. N. Review on nanomaterials: synthesis and applications. *Mater. Today Proc.* **2019**, *18*, 2182–2190.
- (2) (a) Sakthi Devi, R.; Girigoswami, A.; Siddharth, M.; Girigoswami, K. Applications of gold and silver nanoparticles in theranostics. *Appl. Biochem. Biotechnol.* **2022**, *194* (9), 4187–4219. (b) Diez, I.; Ras, R. H. A. Fluorescent silver nanoclusters. *Nanoscale* **2011**, *3*, 1963–1970.
- (3) Bartlett, P. A.; Bauer, B.; Singer, S. Synthesis of water-soluble undecagold cluster compounds of potential importance in electron microscopic and other studies of biological systems. *J. Am. Chem. Soc.* **1978**, *100*, 5085–5089.
- (4) Briant, C. E.; Theobald, B. R. C.; White, J. W.; Bell, L. K.; Mingos, D. M. P.; Welch, A. Synthesis and X-ray structural characterization of the centred icosahedral gold cluster compound  $[\text{Au}_3(\text{PMe}_2\text{Ph})_{10}\text{Cl}_2](\text{PF}_6)_3$ ; the realization of a theoretical prediction. *J. Chem. Soc. Chem. Commun.* **1981**, 201–202.
- (5) Schmid, G.; Pfeil, R.; Boese, R.; Bandermann, F.; Meyer, S.; Calis, G. H. M.; Vandervelden, J. W. A.  $\text{Au}_{55}[\text{P}(\text{C}_6\text{H}_5)_3]_{12}\text{Cl}_6$  — ein Goldcluster ungewöhnlicher Größe. *Chem. Ber.* **1981**, *114*, 3634–3642.
- (6) (a) Zheng, J.; Nicovich, P. R.; Dickson, R. M. Highly fluorescent noble-metal quantum dots. *Annu. Rev. Phys. Chem.* **2007**, *58*, 409–431. (b) Zheng, J.; Petty, J. T.; Dickson, R. M. High quantum yield blue emission from water-soluble  $\text{Au}_8$  nanodots. *J. Am. Chem. Soc.* **2003**, *125*, 7780–7781. (c) Zheng, J.; Zhang, C. W.; Dickson, R. M. Highly fluorescent, water-soluble, size-tunable gold quantum dots. *Phys. Rev. Lett.* **2004**, *93*, 077402. (d) Duan, H.; Nie, S. Etching Colloidal Gold Nanocrystals with Hyperbranched and Multivalent Polymers: A New Route to Fluorescent and Water-Soluble Atomic Clusters. *J. Am. Chem. Soc.* **2007**, *129*, 2412–2413. (e) Habeeb Muhammed, M. A.; Ramesh, S.; Sinha, S. S.; Pal, S. K.; Pradeep, T. Two distinct fluorescent quantum clusters of gold starting from metallic nanoparticles by pH-dependent ligand etching. *Nano Res.* **2008**, *1*, 333–340.
- (7) Sevillano, P.; Fuhr, O.; Hampe, O.; Lebedkin, S.; Matern, E.; Fenske, D.; Kappes, M. M. Synthesis, Characterization, and X-ray Structure Determination of  $[\text{Au}_{18}(\text{P})_2(\text{PPh})_4(\text{PPhPh})(\text{dppm})_6]\text{Cl}_3$ . *Inorg. Chem.* **2007**, *46*, 7294–7298.
- (8) (a) Schaaff, T. G.; Knight, G. M.; Shafiqullin, N.; Borkman, R. F.; Whetten, R. L. Isolation and Selected Properties of a 10.4 kDa Gold: Glutathione Cluster Compound. *J. Phys. Chem. B* **1998**, *102*, 10643–10646. (b) Shichibu, Y.; Negishi, Y.; Tsukuda, T.; Teranishi, T. Large-Scale Synthesis of Thiolated  $\text{Au}_{25}$  Clusters via Ligand Exchange Reactions of Phosphine-Stabilized  $\text{Au}_{11}$  Clusters. *J. Am. Chem. Soc.* **2005**, *127*, 13464–13465. (c) Shichibu, Y.; Negishi, Y.; Tsunoyama, H.; Kanehara, M.; Teranishi, T.; Tsukuda, T. Extremely High Stability of Glutathione-Protected  $\text{Au}_{25}$  Clusters Against Core Etching. *Small* **2007**, *3*, 835–839. (d) Habeeb Muhammed, M. A.; Pradeep, T. Reactivity of  $\text{Au}_{25}$  clusters with  $\text{Au}^{3+}$ . *Chem. Phys. Lett.* **2007**, *449*, 186–190. (e) Shibu, E. S.; Muhammed, M. A. H.; Tsukuda, T.; Pradeep, T. Ligand Exchange of  $\text{Au}_{25}\text{SG}_{18}$  Leading to Functionalized Gold Clusters: Spectroscopy, Kinetics, and Luminescence. *J. Phys. Chem. C* **2008**, *112*, 12168–12176. (f) Muhammed, M. A. H.; Shaw, A. K.; Pal, S. K.; Pradeep, T. Quantum Clusters of Gold Exhibiting FRET. *J. Phys. Chem. C* **2008**, *112*, 14324–14330. (g) Zhu, M.; Lanni, E.; Garg, N. M. E.; Bier, M. E.; Jin, R. Kinetically Controlled, High-Yield Synthesis of  $\text{Au}_{25}$  Clusters. *J. Am. Chem. Soc.* **2008**, *130*, 1138–1139.
- (9) Toikkanen, O.; Ruiz, V.; Ronnholm, G.; Kalkkinen, N.; Liljeroth, P.; Quinn, B. M. Synthesis and stability of monolayer-protected  $\text{Au}_{38}$  clusters. *J. Am. Chem. Soc.* **2008**, *130*, 11049–11055.
- (10) (a) Yanagimoto, Y.; Negishi, Y.; Fujihara, H.; Tsukuda, T. Chiroptical Activity of BINAP-Stabilized Undecagold Clusters. *J. Phys. Chem. B* **2006**, *110*, 11611–11614. (b) Woehle, G. H. M.; Warner, G.; Hutchison, J. E. Ligand Exchange Reactions Yield Subnanometer, Thiol-Stabilized Gold Particles with Defined Optical Transitions. *J. Phys. Chem. B* **2002**, *106*, 9979–9981. (c) Yang, Y.; Chen, S. Surface Manipulation of the Electronic Energy of Subnanometer-Sized Gold Clusters: An Electrochemical and Spectroscopic Investigation. *Nano Lett.* **2003**, *3*, 75–79. (d) Grant, C. D.; Schwartzberg, A. M.; Yang, Y.; Chen, S.; Zhang, J. Z. Ultrafast study of electronic relaxation dynamics in  $\text{Au}_{11}$ nanoclusters. *Chem. Phys. Lett.* **2004**, *383*, 31–34.
- (11) Muhammed, M. A. H.; Verma, P. K.; Pal, S. K.; Kumar, R.; Paul, S.; Omkumar, R. V.; Pradeep, T. Bright, NIR-Emitting  $\text{Au}_{23}$  from  $\text{Au}_{25}$ : Characterization and Applications Including Biolabeling. *Chem.—Eur. J.* **2009**, *15*, 10110–10120.
- (12) (a) Shibu, E. S.; Radha, B.; Verma, P. K.; Bhyrappa, P.; Kulkarni, G. U.; Pal, S. K.; Pradeep, T. Functionalized  $\text{Au}_{22}$  Clusters: Synthesis, Characterization, and Patterning. *ACS Appl. Mater. Interfaces* **2009**, *1*, 2199–2210. (b) Hewitt, M. A.; Hernandez, H.; Johnson, G. E. Light exposure promotes degradation of intermediates and growth of phosphine-ligated gold clusters. *J. Phys. Chem. C* **2020**, *124*, 3396–3402.
- (13) (a) Petty, J. T.; Zheng, J.; Hud, N. V.; Dickson, R. M. DNA-Templated Ag Nanocluster Formation. *J. Am. Chem. Soc.* **2004**, *126*, 5207–5212. (b) Zhang, J. G.; Xu, S. Q.; Kumacheva, E. Photogeneration of Fluorescent Silver Nanoclusters in Polymer Microgels. *Adv. Mater.* **2005**, *17*, 2336–2340. (c) Shen, Z.; Duan, H.; Frey, H. Water-Soluble Fluorescent Ag Nanoclusters Obtained from Multiarm Star Poly(acrylic acid) as “Molecular Hydrogel” Templates. *Adv. Mater.* **2007**, *19*, 349–352. (d) Ledo-Suárez, A.; Rivas, J.; Rodríguez-Abreu, C.; Rodríguez, M.; Pastor, E.; Hernández-Creus, A.; Oseroff, S. B.; Lopez-Quintela, M. A. Facile Synthesis of Stable Subnanosized Silver Clusters in Microemulsions. *Angew. Chem., Int. Ed.* **2007**, *46*, 8823–8827. (e) Narayanan, S. S.; Pal, S. K. Structural and Functional Characterization of Luminescent Silver-Protein Nanobioconjugates. *J. Phys. Chem. C* **2008**, *112*, 4874–4879. (f) Shang, L.; Dong, S. Facile preparation of water-soluble fluorescent silver nanoclusters using a polyelectrolyte template. *Chem. Commun.* **2008**, 1088–1090. (g) Diez, I.; Pusa, M.; Kulmala, S.; Jiang, H.; Walther, A.; Goldmann, A. S.; Muller, A. H. E.; Ikkala, O.; Ras, R. H. A. Color Tunability and Electrochemiluminescence of Silver Nanoclusters. *Angew. Chem., Int. Ed.* **2009**, *48*, 2122–2125.

- (14) Wu, Z.; Lanni, E.; Chen, W.; Bier, M. E.; Ly, D.; Jin, R. High Yield, Large Scale Synthesis of Thiolate-Protected Ag<sub>7</sub> Clusters. *J. Am. Chem. Soc.* **2009**, *131*, 16672–16674.
- (15) Rao, T. U. B.; Pradeep, T. Luminescent Ag<sub>7</sub> and Ag<sub>8</sub> Clusters by Interfacial Synthesis. *Angew. Chem., Int. Ed.* **2010**, *49*, 3925–3929.
- (16) Rao, T. U. B.; Nataraju, B.; Pradeep, T. Ag<sub>9</sub> Quantum Cluster through a Solid-State Route. *J. Am. Chem. Soc.* **2010**, *132*, 16304–16307.
- (17) (a) Wang, J.; Zhao, J.; Ma, G. Extremely concentrated silver nanoparticles stabilized in aqueous solution by bovine serum albumin (BSA). *Nano-Structures & Nano-Objects*; Elsevier, 2019; Vol. 19, p 100349. (b) Dorobantu, L. S.; Fallone, C.; Noble, A. J.; Veinot, J. G.; Ma, G.; Goss, G. G.; Burrell, R. E. Toxicity of silver nanoparticles against bacteria, yeast, and algae. *J. Nanopart. Res.* **2015**, *17*, 172. (c) Schultz, A. G.; Ong, K. J.; MacCormack, T.; Ma, G.; Veinot, J. G.; Goss, G. G. Silver nanoparticles inhibit sodium uptake in juvenile rainbow trout (*Oncorhynchus mykiss*). *Environ. Sci. Technol.* **2012**, *46*, 10295–10301.
- (18) Ge, S.; Zhao, J.-G.; Ma, G.-B. Monochromatic photolysis to generate silver quantum clusters in polymer matrices with efficiently antibio property. *Langmuir* **2020**, *36*, 4088–4097.
- (19) Nies, D. H. Microbial Heavy-Metal Resistance. *Appl. Microbiol. Biotechnol.* **1999**, *51*, 730–750.
- (20) Slawson, R. M.; Van Dyke, M. I.; Lee, H.; Trevors, J. T. Germanium and Silver Resistance, Accumulation, and Toxicity in Microorganisms. *Plasmid* **1992**, *27*, 72–79.
- (21) Morones-Ramirez, J. R.; Winkler, J. A.; Spina, C. S.; Collins, J. J. Silver enhances antibiotic activity against gram-negative bacteria. *Sci. Transl. Med.* **2013**, *5* (190), 190ra81.
- (22) Aoki, T.; Izumi, H.; Aoyagi, S. Fabrication of a micro needle made of biodegradable polymer material. *Mechatronics for Safety Security and Dependability in a New Era*; Elsevier Science, 2007; pp 381–384.
- (23) (a) Wagner, C. D.; Naumkin, A. V.; Kraut-Vass, A.; Allison, J. W.; Powell, C. J.; Rumble, J. R., Jr. *NIST X-ray Photoelectron Spectroscopy Database*, version 3.5 (web version); National Institute of Standards and Technology: Gaithersburg, MD, 2007, (srdata.nist.gov/xps). (b) Huang, W.; Zhai, H.-J.; Wang, L.-S. Probing the Interactions of O<sub>2</sub> with Small Gold Cluster Anions (Au<sub>n</sub><sup>-</sup>, n = 1–7): Chemisorption vs Physisorption. *J. Am. Chem. Soc.* **2010**, *132*, 4344–4351.
- (24) Miller, L. G.; Diep, B. A. Clinical practice: colonization, fomites, and virulence: rethinking the pathogenesis of community-associated methicillin-resistant *Staphylococcus aureus* infection. *Clin. Infect. Dis.* **2008**, *46* (5), 752–760.
- (25) Nataro, J. P.; Kaper, J. B. Diarrheagenic *Escherichia coli*. *Clin. Microbiol. Rev.* **1998**, *11* (1), 142–201.
- (26) Kumaran, S.; Oh, E.; Han, S.; Choi, H. J. Photopolymerizable, universal antimicrobial coating to produce high-performing multifunctional face masks. *Nano Lett.* **2021**, *21*, 5422–5429.
- (27) (a) Quan, F. S.; Rubino, I.; Lee, S. H.; Koch, B.; Choi, H. J. Universal and reusable virus deactivation system for respiratory protection. *Sci. Rep.* **2017**, *7*, 39956. (b) Rubino, I.; Oh, E.; Han, S.; Kaleem, S.; Hornig, A.; Lee, S. H.; Kang, H. J.; Lee, D. H.; Chu, K. B.; Kumaran, S.; Armstrong, S.; Lalani, R.; Choudhry, S., II; Kim, C.; Quan, F. S.; Jeon, B.; Choi, H. J. Salt coatings functionalize inert membranes into high-performing filters against infectious respiratory diseases. *Sci. Rep.* **2020**, *10*, 13875.
- (28) Fabrega, J.; Luoma, S. N.; Tyler, C. R.; Galloway, T. S.; Lead, J. R. Silver nanoparticles: Behaviour and effects in the aquatic environment. *Environ. Int.* **2011**, *37* (2), 517–531.
- (29) Sims, J. M.; Emmer, T. A. *Silver Sutures in Surgery: the Anniversary Discourse before the New York Academy of Medicine, Delivered in the New Building of the Historical Society on November 18, 1857*; Samuel, S., Ed.; William Wood: New York, 1858.
- (30) Tredget, E. E.; Shankowsky, H. A.; Groeneveld, A.; Burrell, R. A. A matched-pair, randomized study evaluating the efficacy and safety of acticoat silver-coated dressing for the treatment of burn wounds. *J. Burn Care Rehabil.* **1998**, *19*, 531–537.
- (31) Woodrow Wilson International Centre for Scholars. Projection Emerging Nanotechnologies website. 1969, <http://www.nanotechproject.org>.
- (32) Harb, M.; Rabilloud, F.; Simon, D.; Rydlo, A.; Lecoultré, S.; Conus, F.; Rodrigues, V.; Felix, C. Optical absorption of small silver clusters: Ag<sub>n</sub> (n=4–22). *J. Chem. Phys.* **2008**, *129*, 194108.
- (33) (a) Julia, F. Ligand-to-Metal Charge Transfer (LMCT) Photochemistry at 3d-Metal Complexes: An Emerging Tool for Sustainable Organic Synthesis. *Chem. Catal. Chem.* **2022**, *14*, No. e202200916. (27 pages) (b) Li, G.; Lei, Z.; Wang, Q. Luminescent Molecular Ag-S Nanocluster [Ag<sub>62</sub>S<sub>13</sub>(SBU<sup>+</sup>)<sub>32</sub>](BF<sub>4</sub>)<sub>4</sub>. *J. Am. Chem. Soc.* **2010**, *132*, 17678–17679. (c) Walter, M.; Akola, J.; Lopez-Acevedo, O.; Jadzinsky, P. D.; Calero, G.; Ackerson, C. J.; Whetten, R. L.; Grönbeck, H.; Hakkinen, H. A unified view of ligand-protected gold clusters as superatom complexes. *Proc. Natl. Acad. Sci. U.S.A.* **2008**, *105* (27), 9157–9162.
- (34) Ma, P.; Su, M.; Li, X.; Liu, C.; Li, Y.; Yao, Q.; Guo, K. Establishment and Application of *Escherichia* Coil Counting Method Based on Spectrophotometer. *Prog. Vet. Med.* **2020**, *41*, 29–33.
- (35) (a) Scheirs, J.; Priddy, D. *Modern Styrenic Polymer Polystyrene and Styrene Copolymers*; John Wiley & Sons, 2003; p 3. (b) Maul, J.; Frushour, B. G.; Eichenauer, J. R.; Ott, K.-H.; Schade, C. *Polystyrene and Styrene Copolymers in Ullmann's Encyclopedia of Industrial Chemistry*; Wiley VCH: Weinheim, 2007.